Synthesis and Characterization of Cobalt Hydroxide, Cobalt Oxyhydroxide, and Cobalt Oxide Nanodiscs

ARTICLE *in* THE JOURNAL OF PHYSICAL CHEMISTRY C · NOVEMBER 2009

Impact Factor: 4.77 · DOI: 10.1021/jp908548f

4 AUTHORS:

Jing Yang
Northwestern Polytechnical University
103 PUBLICATIONS **1,042** CITATIONS
SEE PROFILE

Hongwei Liu
University of Sydney
124 PUBLICATIONS **2,292** CITATIONS
SEE PROFILE

Wayde Martens
Queensland University of Technology
213 PUBLICATIONS **4,804** CITATIONS
SEE PROFILE

Ray L. Frost
Queensland University of Technology
1,229 PUBLICATIONS **21,502** CITATIONS
SEE PROFILE

Synthesis and Characterization of Cobalt Hydroxide, Cobalt Oxyhydroxide, and Cobalt Oxide Nanodiscs

Jing Yang, Hongwei Liu, Wayde N. Martens, and Ray L. Frost*

Inorganic Materials Research Program, School of Physical and Chemical Sciences, Queensland University of Technology, GPO Box 2434, Brisbane Queensland 4001, Australia

Received: September 3, 2009; Revised Manuscript Received: October 15, 2009

Cobalt hydroxide, cobalt oxyhydroxide, and cobalt oxide nanomaterials were synthesized through simple soft chemistry. The cobalt hydroxide displays hexagonal morphology with clear edges 20 nm long. This morphology and nanosize is retained through to cobalt oxide Co_3O_4 through a topotactical relationship. Cobalt oxyhydroxide and cobalt oxide nanomaterials were synthesized through oxidation and low-temperature calcination from the as-prepared cobalt hydroxide. Characterization of these cobalt-based nanomaterials was fully developed, including X-ray diffraction, transmission electron microscopy combined with selected area electron diffraction, scanning electron microscopy, X-ray photoelectron spectroscopy, Raman spectroscopy, and thermal gravimetric analysis. Bonding of the divalent cobalt hydroxide from the oxyhydroxide and oxides by studying their high-resolution XPS spectra for Co $2p_{3/2}$ and O 1s. Raman spectroscopy of the as-prepared $Co(OH)_2$, CoO(OH), and Co_3O_4 nanomaterials characterized each material. The thermal stability of the materials $Co(OH)_2$ and CoO(OH) was established. This research has developed methodology for the synthesis of cobalt oxide and cobalt oxyhydroxide nanodiscs at low temperatures.

Introduction

In recent years, synthesis of inorganic materials with special morphologies has been of significant interest in material science and industry.[1,2] The intrinsic properties of nano- and microcrystals depend not only on their composition but also on their structure, phase, shape, crystallinity, size, and size distribution.[3] Control of size and morphology is currently a key issue in developing functional materials and much effort has been undertaken for upgrading the characteristics of materials.[4] Novel nanomaterials may be based upon boehmite,[5,6] titania,[7] gallium oxyhydroxide,[8,9] cobalt oxyhydroxide,[10,11] and designed clay minerals.[12,13] Because of their high surface area, chemical and thermally stable properties, and mesoporous properties, metal oxides have been extensively used as carriers and support for a variety of industrial catalysts at high and low temperatures. The oxides of cobalt can be employed as catalysts,[14] adsorbents,[15,16] composite materials,[17,18] and ceramics.[19–21]

Transition metal oxides are widely used in the field of heterogeneous catalysis. Cobalt hydroxide, cobalt oxyhydroxide, cobalt oxides, and their derived compounds are especially interesting due to their exceptional physical and chemical properties, which make them promising materials widely applied in rechargeable Li-ion batteries,[22,23] gas sensing,[24] catalysis,[25,26] ionic exchangers,[27] and magnetic materials,[28] and others. The oxides of cobalt are also a crucial precursor in sol−gel technique for preparing high-purity and high-strength monolithic cobalt oxide ceramics for use as substrates for electronic circuits, abrasive grains, high-temperature refractory materials, fibers, and thin films.[29] Cobalt oxide (Co_3O_4) is an important magnetic p-type semiconductor with an indirect band gap of 1.5 eV.[30] Li et al.[31] reported that Co_3O_4 nanotubes, nanorods, and nanoparticles can be used as the anode materials of lithium-ion batteries.[32] While cobalt oxyhydroxide, CoO(OH), is considered as a nonstoichiometric oxyhydroxide and has more oxidation state (Co^{3+}) than Co_3O_4. In recent years, CoO(OH) has been applied as an alternative material for CO detection, to improve Co_3O_4-based gas sensors. Geng et al.[33] synthesized the hierarchical dumbbell-like CoO(OH) nanostructures, which have large active surface areas and exhibited a superior sensitivity to CO at room temperature, as well as good reproducibility and short response/recovery time. These as-prepared CoO(OH) nanostructures could be potential nanosensors. $Co(OH)_2$ itself is well known as an additive of alkaline secondary batteries; it is also an important starting materials of heterogeneous catalysts and precursor for CoO(OH) and Co_3O_4 materials. It is reported that after 4 h calcination at 400 °C, one-dimensional hierarchical Co_3O_4 nanocolumns were obtained from $Co(OH)_2$ prepared through a one-step hydrothermal synthesis with hydrazine hydrate and Na_3PO_4 as morphology directing agents.[34] As a CO oxidation catalyst, Co_3O_4 nanorods were obtained from nanorod-shaped cobalt hydroxide carbonate which was precipitated by reaction of cobalt acetate with sodium carbonate incorporating ethylene glycol.[26] Yang et al.[35] successfully synthesized CoO(OH) hierarchically hollow spheres by nanorods self-assembly through bubble templating. Pauporte[30] reported crystallized CoO(OH) films were deposited by potentiostatic electrolysis. In this work, through a facile soft-chemistry method, $Co(OH)_2$ nanomaterial with hexagonal nanostructure was synthesized. Furthermore, CoO(OH) and Co_3O_4 nanomaterials were produced using the as-prepared $Co(OH)_2$ nanomaterial as a precursor. The size and morphology was successfully kept, their crystallite size is much smaller than those reported in previous research. The resultant $Co(OH)_2$, CoO(OH), and Co_3O_4 materials were systematically studied by XRD, TEM, SEM, XPS, Raman, and thermogravimetric techniques. The aim of this research is to controllably synthesize a series of cobalt hydroxide, oxyhydroxide, and oxide nanomaterials with particular morphology by simple route and to investigate their intrinsic properties for potential applications.

* To whom correspondence should be addressed. E-mail: r.frost@qut.edu.au.

10.1021/jp908548f
Published on Web 11/02/2009

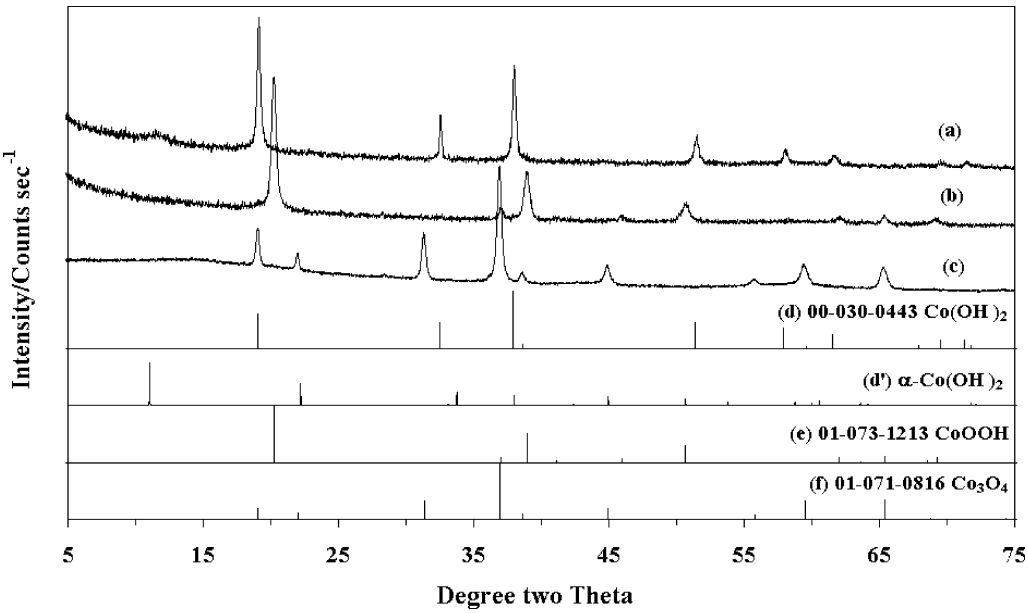

Figure 1. XRD patterns of (a) synthesized $Co(OH)_2$, (b) synthesized CoO(OH), (c) synthesized Co_3O_4, (d) JCPDS card No. 00-030-0443, (d′) α-$Co(OH)_2$ patterns synthesized according to literature, (e) JCPDS card No. 01-073-1213, and (f) JCPDS card No. 01-071-0816.

Experimental Section

Synthesis. In a typical synthesis of $Co(OH)_2$ nanomaterials, 50 mL of 0.1 mol L^{-1} NaOH solution was added dropwise into 80 mL of 0.05 mol L^{-1} $Co(NO_3)_3$ solution, held in a 45 °C sand bath. A pink precipitate was produced, then filtered and washed with deionized water three times. The fresh precipitate was divided into two portions. One half was dried at 65 °C for 2 days, collected as $Co(OH)_2$ product. The other half was dispersed in 20 mL of deionized water under stirring at 45 °C. Then 5 mL of 8 mol L^{-1} NaOH solution was added dropwise together with 2 mL of 30% H_2O_2 solution at 45 °C with stirring. The treated mixture was kept at 45 °C for 18 h. The final brown precipitate was filtered and washed with deionized water three times, then dried at 65 °C for 2 days, collected as CoO(OH). Half of the dried $Co(OH)_2$ sample was then annealed at 400 °C for 4 h to obtain cobalt oxide Co_3O_4.

Characterization

X-ray diffraction. X-ray diffraction patterns were collected using a PANalytical X'Pert PRO X-ray diffractometer (radius: 240.0 mm). Incident X-ray radiation was produced from a line focused PW3373/10 Cu X-ray tube, operating at 40 kV and 40 mA, with Cu Kα radiation of 1.540596 Å. The incident beam passed through a 0.04 rad soller slit, a 1/2° divergence slit, a 15 mm fixed mask, and a 1° fixed antiscatter slit.

SEM. Samples were coated with a thin layer of evaporated gold, and secondary electron images were obtained using a scanning electron microscope (FEI Quanta 200 SEM, FEI Company, Hillsboro, OR). For energy dispersive X-ray spectroscopy (EDXS), the samples were coated with a thin layer of evaporated carbon for conduction and examined in a JEOL 840A analytical SEM (JEOL Ltd., Tokyo, Japan) at 25 kV.

TEM/ SAED. A Philips CM20 transmission electron microscope (TEM) at 160 kV was used to investigate the morphology of the as-prepared samples. All samples were dispersed in absolute ethanol solution and then dropped on copper grids. Selected area electron diffraction (SAED) was performed via the same TEM.

XPS. Data was acquired using a Kratos Axis ULTRA X-ray photoelectron spectrometer incorporating a 165 mm hemispherical electron energy analyzer. The incident radiation was monochromatic Al Kα X-rays (1486.6 eV) at 150 W (15 kV, 10 mA) and at 45° to the sample surface. Photoelectron data was collected at take off angle of $\theta = 90°$. Survey (wide) scans were taken at an analyzer pass energy of 160 eV and multiplex (narrow) high resolution scans of Co 2p, O 1s, and C 1s at pass energy of 20 eV. Survey scans were carried out over 1200−0 eV binding energy range with 1.0 eV steps and a dwell time of 100 ms. Narrow high-resolution scans were run with 0.05 eV steps and 250 ms dwell time. Base pressure in the analysis chamber was 1.0×10^{-9} torr and during sample analysis 1.0×10^{-8} torr.

Atomic concentrations were calculated using the CasaXPS version 2.3.14 software and a linear baseline with Kratos library Relative Sensitivity Factors (RSFs).

A small amount of each finely powdered sample was carefully applied to double-sided adhesive tape on a standard Kratos Axis Ultra sample bar. This was attached to the sample rod of the Load Lock system for initial evacuation to $\sim 1 \times 10^{-6}$ torr. The sample bar was then transferred to the UHV sample analysis chamber (SAC) for collection of X-ray photoemission spectra.

Raman Spectroscopy. Raman spectra were collected using an Olympus BHSM microscope, equipped with 10 and 50× objectives and part of a Renishaw 1000 Raman microscope system, which also includes a monochromator, a filter system, and a charge coupled device (CCD). Raman spectra were excited by a HeNe laser (532 nm) at a resolution of 4 cm^{-1} in the range between 100 and 4000 cm^{-1}. Repeated acquisition using the highest magnification was accumulated to improve the signal-to-noise ratio. Spectra were calibrated using the 520.5 cm^{-1} line of a silicon wafer.

Spectral manipulation such as baseline adjustment, smoothing, and normalization were performed using the software package GRAMS (Galactic Industries Corporation, Salem, NH). Band component analysis was undertaken using the Jandel 'Peakfit' software package which enabled the type of fitting function to be selected and allows specific parameters to be fixed or varied accordingly. Band fitting was done using a Lorentz−Gauss cross-product function with the minimum number of component bands used for the fitting process. The Gauss−Lorentz ratio was

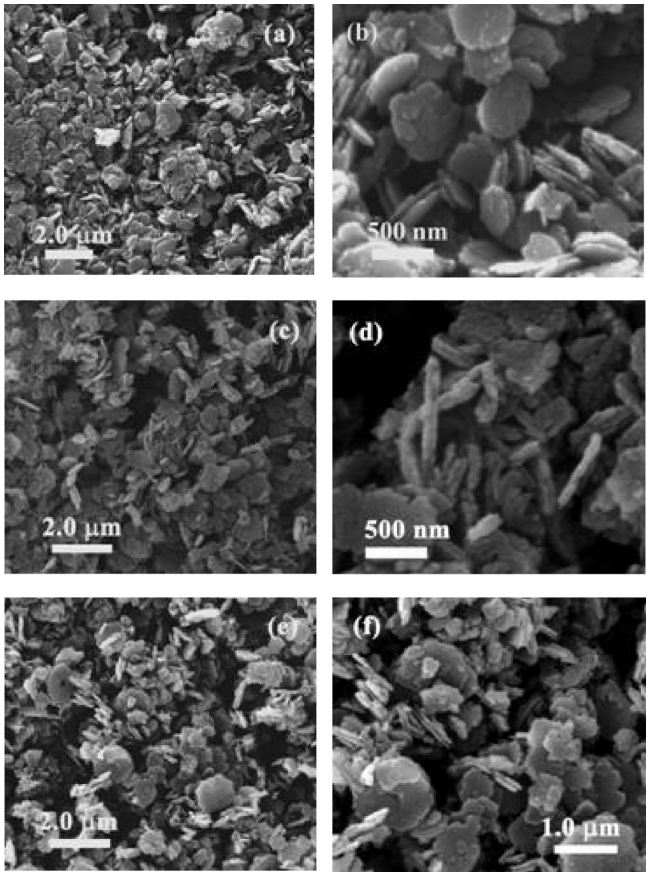

Figure 2. SEM images of (a) $Co(OH)_2$, (b) CoO(OH), and (c) Co_3O_4.

maintained at values greater than 0.7, and fitting was undertaken until reproducible results were obtained with squared correlations of r^2 greater than 0.995.

Thermal Analysis. Thermal decomposition of ~50 mg of sample was carried out in a TA Instruments incorporated high-resolution thermogravimetric analyzer (series Q500) in a flowing nitrogen atmosphere (80 cm^3/min), at a rate of 2.0 °C/min up to 1000 °C. For more information on the experimental and analysis techniques used, refer to previous work by the authors.[36–41]

Results and Discussion

X-ray Diffraction. The X-ray diffraction patterns of the as-prepared cobalt hydroxide, cobalt oxyhydroxide, and cobalt oxide are shown in curves a, b, and c of Figure 1, respectively. It is reported that cobalt hydroxides can crystallize in two polymorphs, α and β. The α-cobalt hydroxides are isostructural with hydrotalcite-like compounds that consist of positively charged $Co(OH)_{2-x}$ layers and charge balancing anions (e.g., NO_3^-, CO_3^{2-}, Cl^-, etc.) in the interlayer gallery, while the β-form is a stoichiometric phase of the composition $Co(OH)_2$ with brucite-like structure and consists of a hexagonal packing of hydroxyl ions with Co(II) occupying alternate rows of octahedral sites. The α-hydroxides thus have a larger interlayer spacing (usually >7 Å, dependent on intercalated anions) than that of the β form (4.6 Å).[42]

All diffraction peaks of the hexagonal cell of brucite-like β-$Co(OH)_2$ can be found in Figure 1a, which are consistent with the peak positions in the literature (JCPDS card, No. 00-030-0443, see Figure 1d). The strong low-angle reflection peak at 19° can be found with *d*-spacing of 4.64 Å, which perfectly

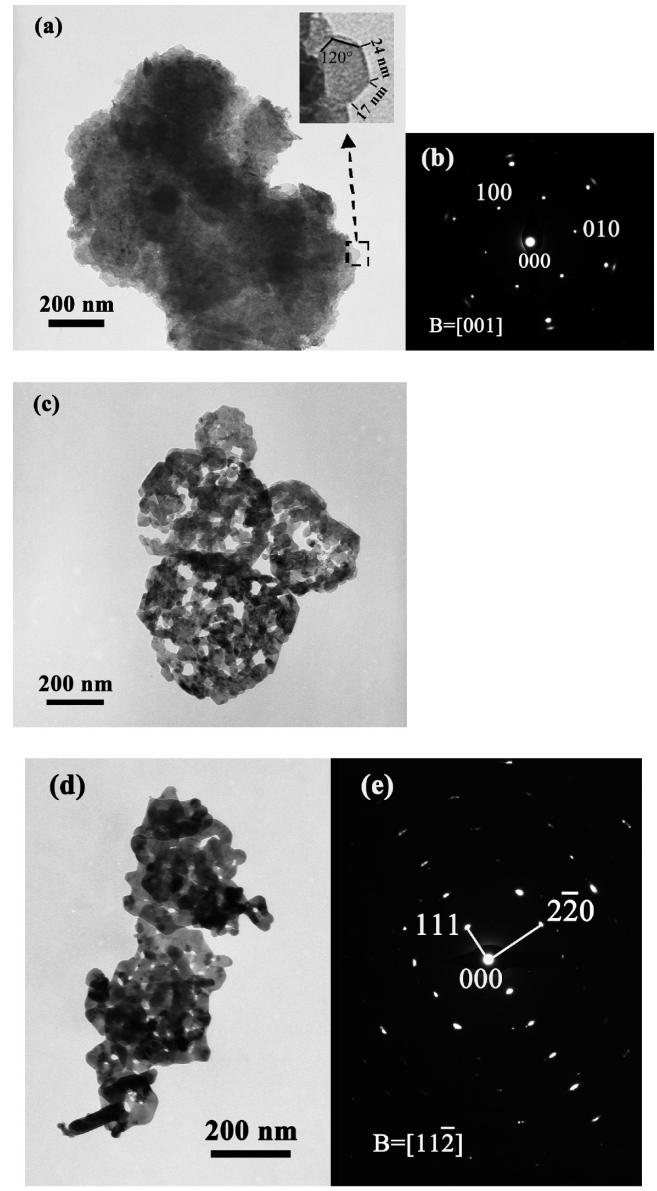

Figure 3. TEM images of (a) $Co(OH)_2$, (c) CoO(OH), and (d) Co_3O_4; SAED patterns of the corresponding particles showing in TEM images: (b) $Co(OH)_2$ and (e) Co_3O_4.

matches the reported interlayer spacing value of β-$Co(OH)_2$.[42] The broad peak with very low intensity at around 10° was assigned to be the trace of α-$Co(OH)_2$ as impurity. (Refer to Figure 1d′, which is a synthesized XRD pattern according to the data reported in the literature.[42]) Figure 1b shows the typical XRD pattern of the as-prepared cobalt oxyhydroxide, CoO(OH) nanomaterials. All the diffraction peaks in this pattern are in good agreement with the standard JCPDS card No. 01-073-1213. No impurity peaks are observed, indicating that the sample oxidized from as-prepared $Co(OH)_2$ with 30% H_2O_2 was pure CoO(OH). The corresponding XRD pattern of the thermally decomposed product from the as-prepared $Co(OH)_2$ nanodiscs is shown as part (c) in Figure 1. It can be observed that all the diffraction peaks in this pattern can be readily indexed to the pure cubic phase of Co_3O_4, which matches well with JCPDS card No. 01-071-0816, indicating that the complete transformation of $Co(OH)_2$ to Co_3O_4 at 400 °C after 4 h. Moreover, all the sharp reflections in these three patterns suggest the high crystalline properties of all the samples. The crystallite size of the synthesized materials was calculated based on Scherrer's

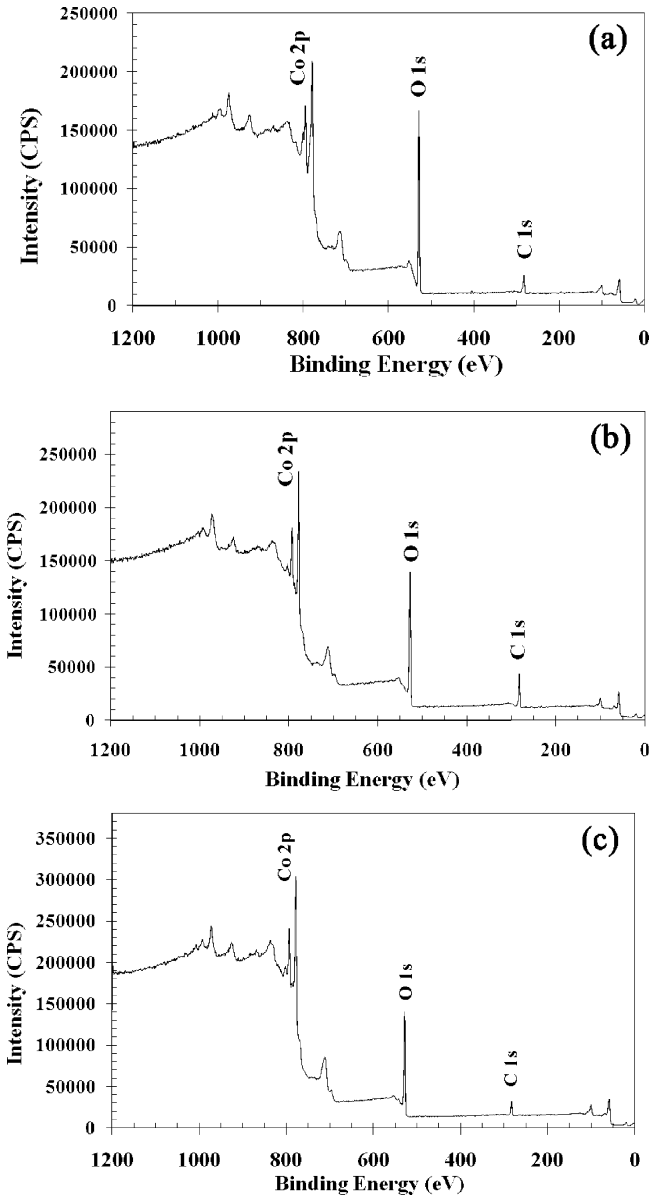

Figure 4. XPS survey spectra of (a) $Co(OH)_2$, (b) CoO(OH), and (c) Co_3O_4.

equation, $D = K\lambda/\beta \cos \theta$. The average crystallite size of $Co(OH)_2$ and CoO(OH) was found both about 40 nm, while the calcined product Co_3O_4 showed a smaller average crystallite size of about 30 nm.

Scanning Electron Microscopy (SEM). The SEM images of the $Co(OH)_2$, CoO(OH), and Co_3O_4 at two magnifications are shown in Figure 2. The compound $Co(OH)_2$ exists as flat platelets in the 100−500 nm range in size. The edges of the platelets appear broken and uneven. This is attribution to a dissolution−reprecipitation process. The platelets appear in pairs. This may be due to a surface-edge charge as is found for kaolinite platelets. An alternative explanation is ascribed in terms of magnetism. The $Co(OH)_2$ platelets are magnetic and the platelets may have a ± relationship. Pralang et al.[43] reported the SEM images of β-$Co(OH)_2$. These images were not as regular as those shown in this work and showed more broken edges. Pralang et al.[43] also investigated the oxidation of $Co(OH)_2$ to CoO(OH). The plate-like doublets were also similar to the Co_3O_4 platelets provided by Cao et al.[44] Shief and Duffy studied the Raman spectra at high pressures and concluded that considerable amorphitisation takes place and because the Raman bands are very broad in the OH stretching region, that a great range of hydrogen bond distances are observed.[45] In some ways this lack of crystallinity and disorder is reflected in the morphology of the $Co(OH)_2$.

The SEM images of CoO(OH) show similar morphology to that of $Co(OH)_2$. The platelets appear smaller and with more broken edges. This may be due to the oxidation of the $Co(OH)_2$, as the oxidation occurs preferentially along certain axes. The SEM images resemble those published by Pralong et al.[43] The regularity of the platelets of $Co(OH)_2$ is retained in the morphology of the Co_3O_4. This shows there is a topotactical relationship between the $Co(OH)_2$ nanoparticles and the Co_3O_4 nanoparticles. The plate-like morphology is retained in the Co_3O_4 plates which retain the double plate patterns of the $Co(OH)_2$.

TEM and SAED. The synthetic cobalt hydroxide $Co(OH)_2$ compound is a pink powder, the particles of which are observed by TEM as aggregated hexagonal thin platelets (Figure 3a). On the edge of the aggregate shown as the insert of Figure 3a, it can be easily seen the thin platelets take hexagonal morphology with clear edge and regular angles of 120° between adjacent sides. The observed edge length of the single hexagonal platelet is around 20 nm, thus 40 nm in size, which is in harmony with the calculation results of Scherrer equation from the X-ray diffraction patterns. In this work we have synthesized very small nanoplatelets. Previous workers manufactured hexagonal plates on the micrometer scale, as opposed to the nanoscale in this work. Because of the nanosize of the platelets, it is difficult to separate these platelets. This size of the hexagonal thin platelets is much smaller than that (120 nm) reported by Geng et al.[46] Because of the strong interfacial tension among these small-size nanoplatelets, they are not easily to be separated as single platelets, even after 1 h sonication. In Figure 3b, the corresponding SAED pattern of the aggregated particle shows 6-fold symmetric feature, which can be readily indexed with the lattice parameters of the phase cobalt hydroxide $Co(OH)_2$. This result reveals the same orientation of the nanoplatelets in the aggregate, with the platelets lying on their (001) crystal planes and the SAED patterns were taken along the 001 zone axis direction. This SAED pattern matches the SAED image of a single cobalt hydroxide particle with typical hexagonal morphology taken by Figlarz et al.[47]

A representative TEM image of as-prepared CoO(OH) is shown in Figure 3c. Hexagonal nanoplatelet fragments are observed in the product, the major being irregular nanoplatelets, which correspond with its SEM images showing more broken-down discs with small holes on the surface. It was reported by Figlarz and co-workers[47] that as the oxidation progresses, the particle habit is broken up. In this TEM image, small irregular nanoplatelets are aggregated to form subcircular particles (100−600 nm in dimension), which is consistent with the SEM measurements. Because of the crystallite multiorientation shown by the irregularly stacking nanoplatelets, the SAED of this as-prepared CoO(OH) shows continuous rings instead of points.

Figure 3d shows the morphology of the product annealed from as-prepared $Co(OH)_2$ at 400 °C for 4 h, where one can see that the aggregated platelet structures are retained. The SAED (Figure 3e) pattern of such a cluster gives a single crystal pattern, showing a well-defined crystalline structure of the face-centered cubic Co_3O_4 phase. The diffraction spot with a lattice spacing of 4.6 Å, corresponding to the value of the (111) plane, while

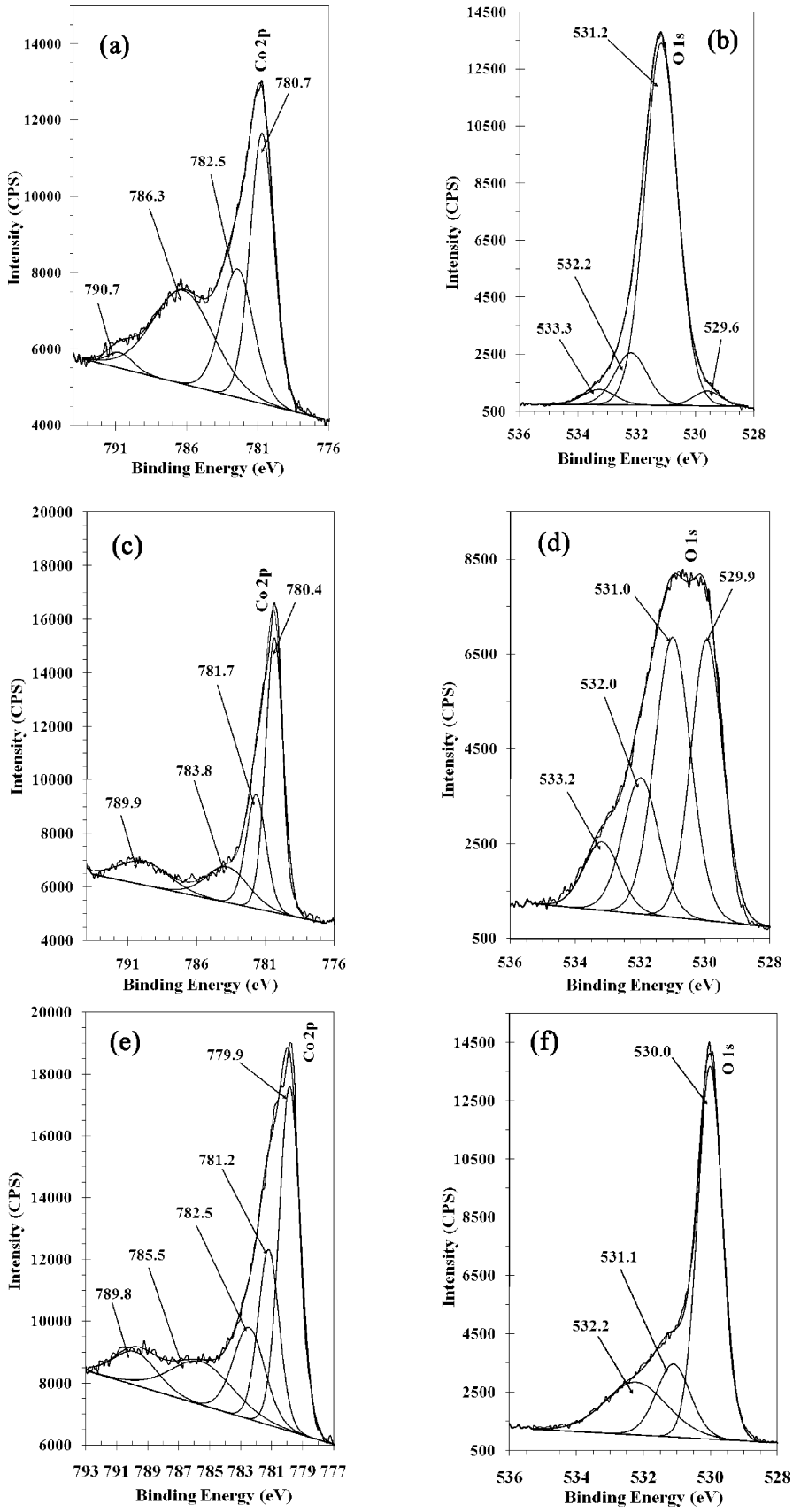

Figure 5. XPS high-resolution spectra of (a) $Co(OH)_2$, (b) CoO(OH), and (c) Co_3O_4.

the spot with a lattice spacing of 2.8 Å correspond to the (2-20) plane.

X-ray Photoelectron Spectroscopy (XPS). XPS is a proven reliable method for intensive investigation for the oxidation state of atoms in the top few layers of material surfaces with partially filled valence bonds. XPS was applied to the study of the chemical states of compounds used in this study. The complete survey spectra of the three synthesized nanomaterials are

TABLE 1: Curve-Fitted XPS Binding Energies of As-Prepared Cobalt Hydroxide, Cobalt Oxyhydroxide, and Cobalt Oxide Nanomaterials

Co $2p_{3/2}$ (eV)			O 1s (eV)		
$Co(OH)_2$	CoOOH	Co_3O_4	$Co(OH)_2$	CoOOH	Co_3O_4
780.7	780.4	779.9	529.6	529.9	530.0
	781.7	781.2	331.2	531.0	531.1
782.5		782.5	532.2	532.0	532.2
	783.8		533.3	533.2	
786.3		785.5			
790.7	789.9	789.8			

displayed in Figure 4. In each of these survey spectra, the main peaks can be clearly indexed to Co 2p, O 1s, and C 1s regions, indicating that no other metallic or inorganic contaminants are present. The high-resolution XPS spectra of Co 2p and O 1s of the synthesized cobalt hydroxide, cobalt oxyhydroxide, and cobalt oxide nanomaterials are compared in Figure 5. All the spectra were referenced to the aliphatic carbon at binding energy (BE) of 285.0 eV.

High-resolution Co 2p spectrum show spin−orbit splitting into $2p_{1/2}$ and $2p_{3/2}$ components, and both components qualitatively contain the same chemical information.[48] Therefore, in this study, only the higher-intensity Co $2p_{3/2}$ bands were curve-fitted, including the shake-up satellites of the cobalt ions. Artyushkova et al.[48] applied Principal Component Analysis to analyze the results quantitatively from the curve-fitted spectra of pure elements and various combinations of elements. This provides the basis of identifying all chemical species despite significant overlaps in binding energy. Figure 5a, c, and e presents the curve-fitted Co $2p_{3/2}$ spectra for $Co(OH)_2$, CoO(O)H, and Co_3O_4. The intensive main peaks are at 780.7 eV for $Co(OH)_2$, 780.4 eV for CoO(OH) and 779.9 eV for Co_3O_4, showing slight decrease in binding energy, though not much. Moreover, another Co $2p_{3/2}$ was fitted at 782.5 eV for $Co(OH)_2$, while this peak shifted to lower BE in the spectrum of CoO(OH). Interestingly, these two peaks are both observed in the spectrum of Co_3O_4, which contains Co(II) and Co(III) two oxidation state. The fact that chemical shift occurred from 782.5 eV for $Co(OH)_2$ to 781.7 eV for CoO(OH) and that Co_3O_4 presents peaks at 782.5 and 781.2 eV can be considered as evidence for distinguishing the divalent oxide from its hydroxides with the same retained morphology.

In the higher BE region, two peaks are required to fit as the satellites for each nanomaterial. In addition to the normal core photoelectron lines, satellite line structure always can be observed in the late 3d transition metal compounds. These additional spectral lines have been related either to a coupling between unpaired electrons in the atom (multiplet splitting) or a multiple electron excitation (the so-called 'shakeup').[49] Spectral results from the interaction with metal valence electrons can provide chemical environment information about the metal ions. It is reported that cobalt(III) oxides were distinguished from cobalt(II) oxides by the absence of mulitelectron excitation satellites in the former.[49] This finding is confirmed by our study. In Figure 5a, a broad satellite peak at 786.3 eV was found for $Co(OH)_2$, which is missing in the spectrum of CoO(OH), while in the spectrum of Co_3O_4 this satellite decrease in intensity and shifted to lower BE, at 785.5 eV. However, these three cobalt compounds all retain a lower satellite at around 789.9 eV.

In the high-resolution XPS spectra, O 1s bands are often complex; however, their decomposition can reveal all the component peaks. The peaks of the O 1s XPS spectra can be fitted and interpreted accordingly. This provides a database of values for the O 1s XPS spectra. XPS spectra may be fitted in different ways and this may affect the interpretation of the XPS data. Studies were performed on simple compounds to obtain reference data for the proper peak assignment. In this study, as shown in Figure 5d, four peaks are required to curve fit the O 1s XPS broadband for cobalt oxyhydroxide. Two intense bands at 531.0 and 529.9 eV are clearly observed, which are considered to be the O from the OH and oxide ions. O from hydroxides is on the higher BE side of the peak, corresponding to the oxide ions.[50] The qualitative analysis also showed that these two kinds of oxygen obtained similar ratio in the compound of CoO(OH), which is consistent with their atom ratio of 1:1. These curve-

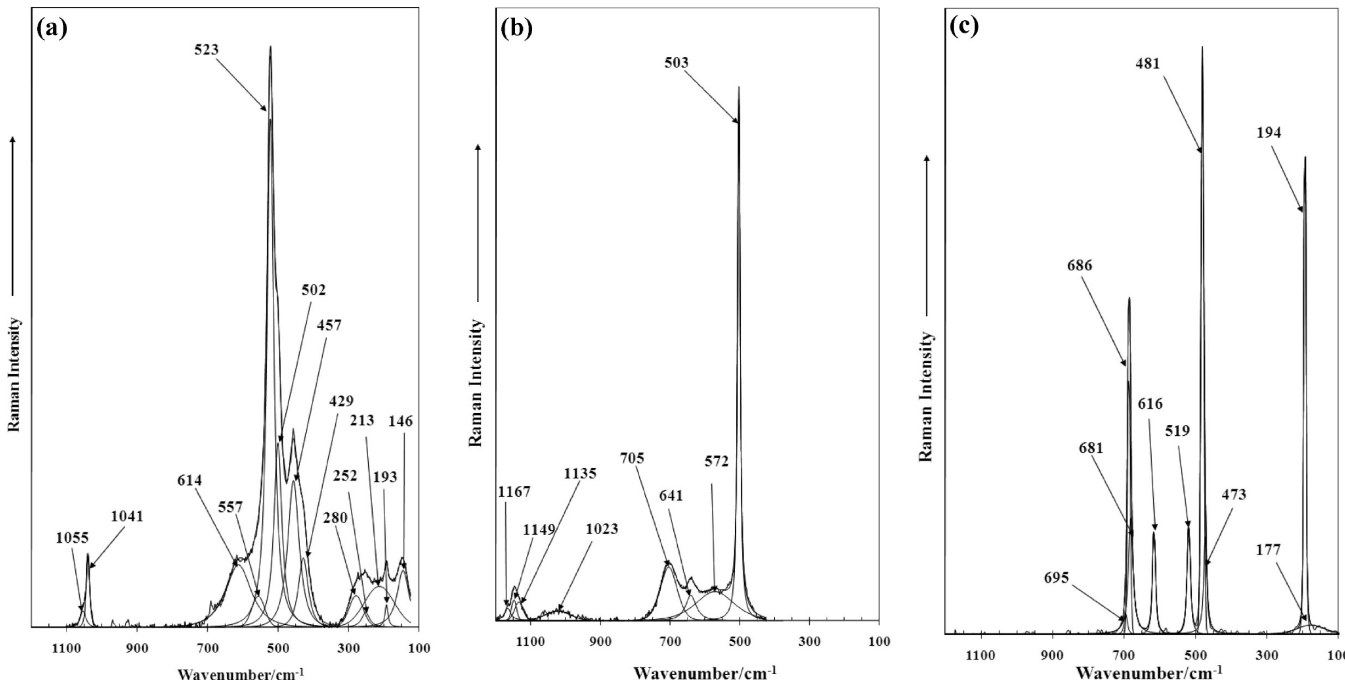

Figure 6. Raman spectra of (a) $Co(OH)_2$ (b) CoO(OH), and (c) Co_3O_4 in the 100−1200 cm^{-1} region.

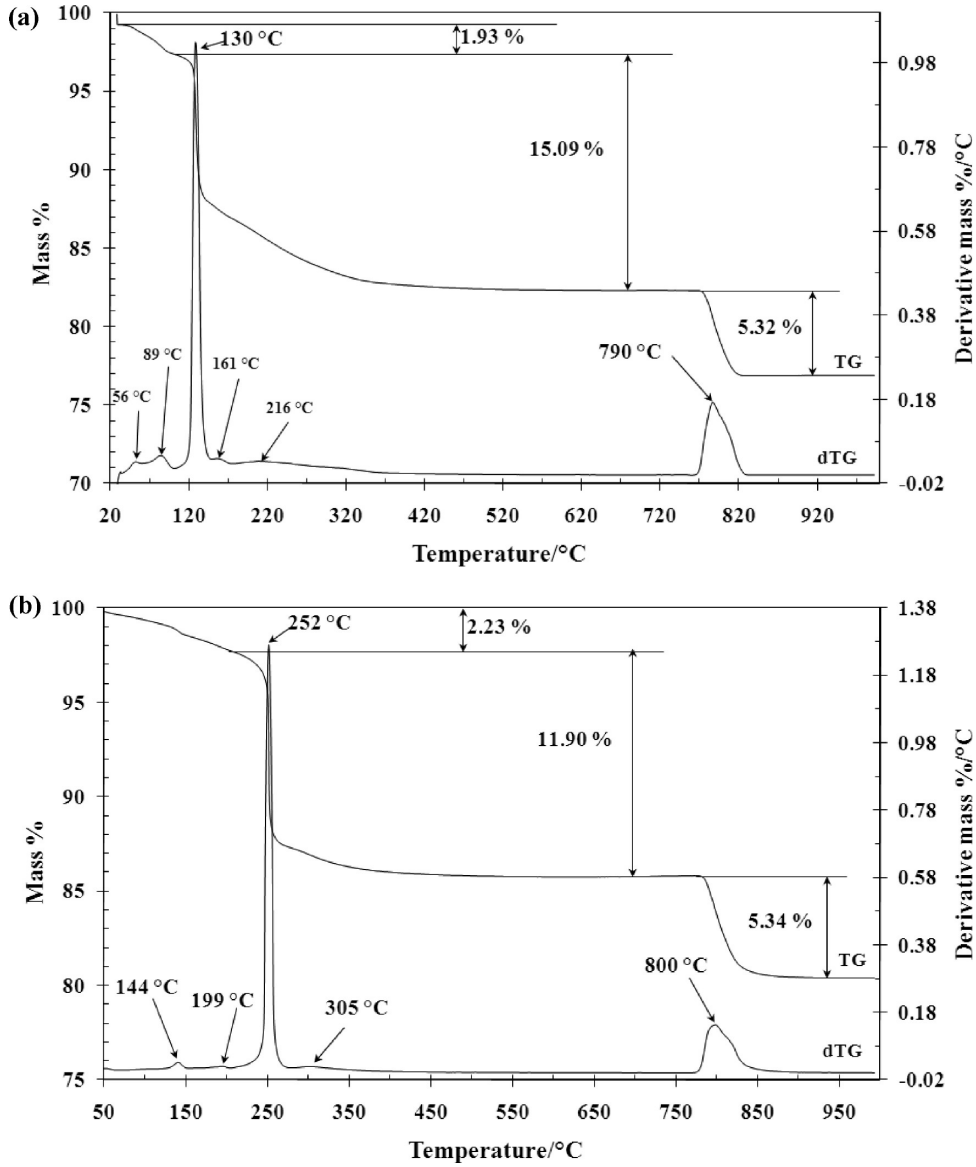

Figure 7. Thermal analysis of (a) $Co(OH)_2$ and (b) CoO(OH).

fitted band positions for the main peaks in O 1s spectrum of CoO(OH) agree perfectly with the XPS study for $Co(OH)_2$ containing hydroxyl only and Co_3O_4 only with oxide ions. Figure 5b presents the high resolution O 1s of cobalt hydroxide, with a main peak at 531.2 eV which matches with the 531.0 eV peak in CoO(OH) spectrum. While in Figure 5f for O 1s spectrum of cobalt oxide, a sharp peak at 530.0 eV can be observed, which is in good agreement with the main peak shown in O 1s spectrum of cobalt oxyhydroxide. In Table 1 the curve-fit results for all the Co $2p_{3/2}$ and O 1s spectra are presented. Low peaks in the spectra are ascribed to hydroxyl and carbonate ions contamination on the surface of the sample. Stoch and Gablankowska-Kukucz[50] studied the XPS of carbonates formed on oxide surfaces for the O 1s band and compared reported O 1s XPS binding energies of cobalt and lanthanum compounds. These researchers found O 1s BE for lattice oxide ions O^{2-} was in the rather narrow range around 529.7 eV; for hydroxide ions OH^-, 531.0 eV was found for $Co(OH)_2$.[51] As far as we know, no previous work made so detailed comparison and discussion on the XPS study for Co $2p_{3/2}$ and O 1s spectra of $Co(OH)_2$, CoO(OH), and Co_3O_4 nanomaterials.

Raman Spectroscopy. The Raman spectra of the $Co(OH)_2$, CoO(OH), and Co_3O_4 are displayed in panels a, b, and c of Figures 6, respectively. These spectra report the Raman spectroscopy of the nanomaterials as shown in Figure 2. The results of the Raman spectral analysis are reported in Table S1 (see Supporting Information). Included in this table are the results from other published papers.[52–55] The Raman spectrum of $Co(OH)_2$ is dominated by an intense highly polarized band at 523 cm^{-1}. This band is attributed to the CoO (A_g) symmetric stretching mode. The Raman spectra of $Co(OH)_2$ at high pressures has been published.[45] Mockenhaupt et al. reported a Raman band at 522 cm^{-1} and assigned the band to an OH deformation mode. However, such an assignment seems improbable. These workers also identified an infrared band at the same position (522 cm^{-1} assigned to the E_u mode). Bockman et al.[52] studied coatings of $Co(OH)_2$ on various substrates and measured Raman maps of the surfaces. The major band was found at 515 cm^{-1}; no band assignments were given in this publication. The position of the band attributed to $Co(OH)_2$ was found to be dependent upon the substrate and the method of coating and the position was found to vary according to the amount of deposited $Co(OH)_2$. The second most intense band is observed at 457 cm^{-1} and is assigned to an OCoO bending mode. This band was observed at 426 cm^{-1} in the infrared spectrum of $Co(OH)_2$ as reported by Mockenhaupt et al.[54] This

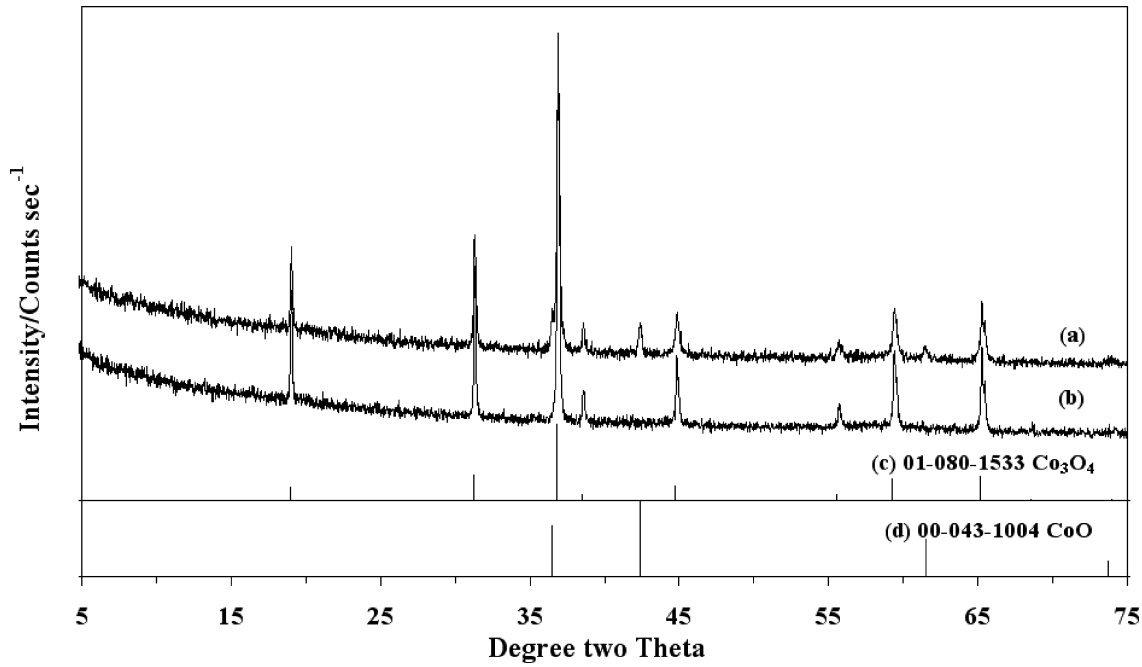

Figure 8. XRD patterns of the thermal products after TG study: (a) from $Co(OH)_2$ and (b) from CoO(OH). XRD patterns from literature: (c) JCPDS card No. 01-080-1533 and (d) JCPDS card No. 00-043-1004.

band appears as a shoulder in our Raman spectrum. Bockman et al.[52] also reported a Raman band at 470 cm^{-1} for high $Co(OH)_2$ content. Two Raman bands are observed at 1041 and 1055 cm^{-1}. These bands are assigned to the OH deformation modes. Such bands are normally of low intensity in the Raman spectra and are more intense in the infrared spectra, yet such bands were not reported in the infrared spectra obtained by Mockenhaupt et al.[54] It is proposed that there are three forms of $Co(OH)_2$ which may be labeled as α-$Co(OH)_2$, β-$Co(OH)_2$, and γ-$Co(OH)_2$. These compounds are isomorphous, having the same formula but different crystalline structures. Evidence for this polymorphism is based upon the polymorphism of the naturally occurring mineral CoO(OH) known as heterogenite. The Raman spectrum obtained for $Co(OH)_2$ depends upon which structure is being analyzed. This is why there are three different spectra published in the literature. A comparison may be made with FeO(OH) where three different crystalline forms exist namely goethite (α-$Fe(OH)_2$), lepidocrocite (β-$Fe(OH)_2$), and feroxyhyte (γ-$Fe(OH)_2$).

The obtained Raman spectrum of the synthesized CoO(OH) (Figure 6b) displays peaks at 503, 572, 641, 705, 1023, and 1149 cm^{-1}. These values correspond precisely with the values published by Pauporte et al. The authors tabulated the most intense peaks at 503 and 635 cm^{-1}. These authors studied the variation in peak position with temperature. At low temperatures the CoO(OH) underwent a phase change to Co_3O_4. The values differ from those published by Tang et al. and Bockman et al.[52,55] The difference may be due to polymorphism. Tang et al.[55] reported the spectrum of CoO(OH). Raman bands were found at 367, 482, 599, and 809 cm^{-1} and an infrared band at 584 cm^{-1} which was assigned to the CoO stretching vibration. The compound CoO(OH) is a naturally occurring mineral known as heterogenite and occurs in at least three different polytypes (1R, 3R, and 2H). The Raman spectrum of this mineral displays three bands at 492, 620, and 855 cm^{-1}. The infrared spectrum of this mineral shows bands at 560, 727, 875, and 1427 cm^{-1}. The values for the Raman peaks of heterogenite differ from those reported by Tang et al.[55]

The Raman spectrum of the phase Co_3O_4 (Figure 6c) displays intense bands at 194, 481, and 686 cm^{-1} with bands of lesser intensity at 519 and 616 cm^{-1}. The Raman band at 686 cm^{-1} is highly polarized. On the basis of the work of Hadjiev et al.[53] the bands are assigned as follows. The 686 cm^{-1} band to A_{1g} mode, the 616 cm^{-1} the F_{2g} mode, the band at 519 cm^{-1} the F_{2g} mode, the band at 481 cm^{-1} the E_g mode, and the band at 194 cm^{-1} the F_{2g} mode. Tang et al.[55] reported infrared bands at 570 and 661 cm^{-1} and Raman bands at 482, 519, 621, and 690 cm^{-1}. Some of the bands as identified in the so-called cobalt cements as reported by Bockman et al.[52] at 515 and 685 cm^{-1} are better assigned to Co_3O_4 rather than $Co(OH)_2$ as defined by their Raman spectra.

Thermal Analysis. There have been several studies on the morphological and topotactical changes of the reaction of $Co(OH)_2$ to CoO(OH) and CoO(OH) to Co_3O_4.[43,47,56] Figlarz et al. found that $Co(OH)_2$ decomposed to both CoO(OH) and Co_3O_4 simultaneously.[47] Tang et al. also more recently reported the thermal decomposition of these compounds.[55] The thermal analysis of $Co(OH)_2$ and CoO(OH) are reported in panels a and b of Figure 7, respectively. The major mass loss step occurs at 130 °C with a mass loss of 15.09%. This mass loss step is attributed to the dehydroxylation of the compound according to the reaction $6Co(OH)_2 + O_2 \rightarrow 2Co_3O_4 + 6H_2O$. XRD shows that the product of the thermal decomposition is mainly Co_3O_4 in Figure 8a. Minor mass losses observed at 56 and 89 °C are attributed to the desorption of water. The very minor mass loss steps at 161 and 216 °C are ascribed to impurities. A second mass loss step is observed at 790 °C and is attributed to the formation of CoO through loss of oxygen according to the reaction $2Co_3O_4 \rightarrow 6CoO + O_2$. CoO was found from the X-ray diffraction study of the products of the thermal decomposition (Figure 8a). The experimentally determined mass loss of 15.09% may be compared with the theoretical mass loss of 19.3%. The TG pattern of the compound CoO(OH), as reported in Figure 7b, shows that CoO(OH) decomposes at 252 °C. The thermal decomposition reaction is $12CoO(OH) \rightarrow 4Co_3O_4 + O_2 + 6H_2O$. A higher temperature mass loss is observed at 800 °C

with a mass loss of 5.34%. The reaction is the same as for $Co(OH)_2$ thermal decomposition: the reaction $2Co_3O_4 \rightarrow 6CoO + O_2$. X-ray diffraction shows that the product of the thermal decomposition is Co_3O_4 in Figure 8b. The theoretical mass loss for this step is 6.639%, which is slightly greater than the experimentally determined value of 5.32%. Tang et al.[55] reported the thermal decomposition of Co_3O_4 at 820 °C which is in good agreement with the decomposition steps observed for $Co(OH)_2$ and CoO(OH) at 790 and 800 °C reported in this work.

Conclusions

The synthesized cobalt hydroxide, oxyhydroxide, and oxide nanomaterials were obtained by soft-chemistry methods. A combination of techniques were used to study morphology and structure of the as-prepared materials, including XRD, SEM, TEM, XPS, Raman spectroscopy, and thermal analysis. The synthetic cobalt hydroxide was identified as the β form with a brucite-like structure and was successfully oxidized to cobalt oxyhydroxide with 30% H_2O_2 and annealed to cobalt oxide at low temperature. These three cobalt compounds retain the topotactical relationship in structure. XPS spectra of the as-prepared cobalt hydroxide, oxyhydroxide, and oxide nanomaterials have been studied with a view to determining spectral characteristics to allow the identification of each species. Raman spectroscopy is proved as a facile way to provide information on structure of the synthesized compounds. The dehydroxylation of the synthetic cobalt hydroxide happened at 130 °C, while cobalt oxyhydroxide decomposed at 252 °C.

Acknowledgment. The financial and infrastructure support of the Queensland University of Technology Inorganic Materials Research Program of the School of Physical and Chemical Sciences are gratefully acknowledged. J.Y. thanks the Queensland University of Technology for a postgraduate doctoral scholarship.Thanks are also given to Dr. B. Wood for technical and computing support in the XPS study.

Supporting Information Available: Table of Raman data. This material is available free of charge via the Internet at http://pubs.acs.org.

References and Notes

(1) Fendler, J. H.; Meldrum, F. C. *Advanced Materials*; Weinheim: Germany, 1995; Vol. 7, p 607.
(2) Lakshmi, B. B.; Patrissi, C. J.; Martin, C. R. *Chem. Mater.* **1997**, *9*, 2544.
(3) Sun, Y.; Xia, Y. *Nature* **2002**, *298*, 2176.
(4) Gudiksen, M. S.; Lauhon, L. J.; Wang, J.; Smith, D. C.; Lieber, C. M. *Nature* **2002**, *415*, 617.
(5) Yang, J.; Frost, R. L.; Yuan, Y. *Thermochim. Acta* **2009**, *483*, 29.
(6) Yang, J.; Zhao, Y.; Frost, R. L. *Appl. Surf. Sci.* **2009**, *255*, 7925.
(7) Yang, X.; Yang, D.; Zhu, H.; Liu, J.; Martins, W. N.; Frost, R.; Daniel, L.; Shen, Y. *J. Phys. Chem. C* **2009**, *113*, 8243.
(8) Zhao, Y.; Frost, R. L. *J. Raman Spectrosc.* **2008**, *39*, 1494.
(9) Zhao, Y.; Frost, R. L.; Yang, J.; Martens, W. N. *J. Phys. Chem. C* **2008**, *112*, 3568.
(10) Zhang, L.; Dutta, A. K.; Jarero, G.; Stroeve, P. *Langmuir* **2000**, *16*, 7095.
(11) Hou, Y.; Kondoh, H.; Shimojo, M.; Kogure, T.; Ohta, T. *J. Phys. Chem. B* **2005**, *109*, 19094.
(12) Daniel, L. M.; Frost, R. L.; Zhu, H. Y. *J. Colloid Interface Sci.* **2008**, *321*, 302.
(13) Daniel, L. M.; Frost, R. L.; Zhu, H. Y. *J. Colloid Interface Sci.* **2008**, *322*, 190.
(14) Le Loarer, J.-L.; Nussbaum, H.; Bortzmeyer, D. Alumina extrudates, methods for preparing and use as catalysts or catalyst supports; (Rhodia Chimie, Fr.). Application: WO, 1998; p 44.
(15) Burkat, V. S.; Dudorova, V. S.; Smola, V. S.; Chagina, T. S. *Light Metals*; TMS: Warrendale, PA, 1985; p 1443.
(16) Nedez, C.; Boitiaux, J.-P.; Cameron, C. J.; Didillon, B. *Langmuir* **1996**, *12*, 3927.
(17) Chen, Y.; Jin, L.; Xie, Y. *J. Sol−Gel Sci. Technol.* **1998**, *13*, 735.
(18) Xue, D. S.; Huang, Y. L.; Ma, Y.; Zhou, P. H.; Niu, Z. P.; Li, F. S.; Job, R.; Fahrner, W. R. *J. Mater. Sci. Lett.* **2003**, *22*, 1817.
(19) Philipse, A. P.; Nechifor, A.-M.; Patmamanoharan, C. *Langmuir* **1994**, *10*, 4451.
(20) Okada, K.; Tanaka, A.; Hayashi, S.; Daimon, K.; Otsuka, N. *J. Mater. Res.* **1994**, *9*, 1709.
(21) Ananthakumar, S.; Raja, V.; Warrier, K. G. K. *Mater. Lett.* **2000**, *43*, 174.
(22) Chen, J.-M.; Hsieh, C.-T.; Huang, H.-W.; Huang, Y.-H.; Lin, H.-H.; Liu, M.-H.; Liao, S.-C.; Shih, H.-C. Synthesis of composite nanofibers for applications in lithium batteries; (Taiwan). Application: US US, 2008; p 12.
(23) Kim, I.-D.; Hong, J.-M.; Jo, S.-M. Anode material with nanofiber structure for secondary batteries; (S. Korea). Application: US US, 2008; p 23.
(24) Frost, R. L.; Wain, D. *J. Therm. Anal. Calorim.* **2008**, *91*, 267.
(25) Lai, T.-L.; Lai, Y.-L.; Lee, C.-C.; Shu, Y.-Y.; Wang, C.-B. *Catal. Today* **2008**, *131*, 105.
(26) Xie, X.; Li, Y.; Liu, Z.-Q.; Haruta, M.; Shen, W. *Nature (London)* **2009**, *458*, 746.
(27) Liu, Z.; Ma, R.; Osada, M.; Iyi, N.; Ebina, Y.; Takada, K.; Sasaki, T. *J. Am. Chem. Soc.* **2006**, *128*, 4872.
(28) Zhang, Y.; Chen, Y.; Wang, T.; Zhou, J.; Zhao, Y. *Microporous Mesoporous Mater.* **2008**, *114*, 257.
(29) Kaya, C.; He, J. Y.; Gu, X.; Butler, E. G. *Microporous Mesoporous Mater.* **2002**, *54*, 37.
(30) Pauporte, T.; Mendoza, L.; Cassir, M.; Bernard, M. C.; Chivot, J. *J. Electrochem. Soc.* **2005**, *152*, C49.
(31) Li, w.-Y.; Xu, L.-N.; Chen, J. *Adv. Funct. Mater.* **2005**, *15*, 851.
(32) Pauporte, T.; Mendoza, L.; Cassir, M.; Bernard, M. C.; Chivot, J. *J. Electrochem. Soc.* **2005**, *152*, C49.
(33) Geng, B.; Zhan, F.; Jiang, H.; Xing, Z.; Fang, C. *Cryst. Growth Des.* **2008**, *8*, 3497.
(34) Shao, Y.; Sun, J.; Gao, L. *J. Phys. Chem. C* **2009**, *113*, 6566.
(35) Yang, J. H.; Sasaki, T. *Chem. Mater.* **2008**, *20*, 2049.
(36) Frost, R. L.; Hales, M. C.; Martens, W. N. *J. Therm. Anal. Calorim.* **2009**, *95*, 999.
(37) Palmer, S. J.; Spratt, H. J.; Frost, R. L. *J. Therm. Anal. Calorim.* **2009**, *95*, 123.
(38) Frost, R. L.; Locke, A. J.; Hales, M. C.; Martens, W. N. *J. Therm. Anal. Calorim.* **2008**, *94*, 203.
(39) Vagvoelgyi, V.; Daniel, L. M.; Pinto, C.; Kristof, J.; Frost, R. L.; Horvath, E. *J. Therm. Anal. Calorim.* **2008**, *92*, 589.
(40) Vagvolgyi, V.; Frost, R. L.; Hales, M.; Locke, A.; Kristof, J.; Horvath, E. *J. Therm. Anal. Calorim.* **2008**, *92*, 893.
(41) Vagvolgyi, V.; Hales, M.; Martens, W.; Kristof, J.; Horvath, E.; Frost, R. L. *J. Therm. Anal. Calorim.* **2008**, *92*, 911.
(42) Liu, Z.; Ma, R.; Osada, M.; Takada, K.; Sasaki, T. *J. Am. Chem. Soc.* **2005**, *127*, 13869.
(43) Pralong, V.; Delahaye-Vidal, A.; Beaudoin, B.; Gerand, B.; Tarascon, J. M. *J. Mater. Chem.* **1999**, *9*, 955.
(44) Cao, A.-M.; Hu, J.-S.; Liang, H.-P.; Song, W.-G.; Wan, L.-J.; He, X.-L.; Gao, X.-G.; Xia, S.-H. *J. Phys. Chem. B* **2006**, *110*, 15858.
(45) Shieh, S. R.; Duffy, T. S. *Phys. Rev. B: Condens. Matter Mater. Phys.* **2002**, *66*, 134301/1.
(46) Geng, B.; Zhan, F.; Fang, C.; Yu, N. *J. Mater. Chem.* **2008**, *18*, 4977.
(47) Figlarz, M.; Guenot, J.; Tournemolle, J. N. *J. Mater. Sci.* **1974**, *9*, 772.
(48) Artyushkova, K.; Levendosky, S.; Atanassov, P.; Fulghum, J. *Top. Catal.* **2007**, *46*, 263.
(49) McIntyre, N. S.; Cook, M. G. *Anal. Chem.* **1975**, *47*, 2208.
(50) Stoch, J.; Gablankowska-Kukucz, J. *Surf. Interface Anal.* **1991**, *17*, 165.
(51) Haber, J.; Stoch, J.; Ungier, L. *J. Electron Spectrosc. Relat. Phenom.* **1976**, *9*, 459.
(52) Bockman, O.; Ostvold, T.; Voyiatzis, G. A.; Papatheodorou, G. N. *Hydrometallurgy* **2000**, *55*, 93.
(53) Khadzhiev, V.; Iliev, M.; Vergilov, I. *J. Phys. C: Solid State Phys.* **1988**, *21*, L199.
(54) Mockenhaupt, C.; Zeiske, T.; Lutz, H. D. *J. Mol. Struct.* **1998**, *443*, 191.
(55) Tang, C.-W.; Wang, C.-B.; Chien, S.-H. *Thermochim. Acta* **2008**, *473*, 68.
(56) Figlarz, M.; Guenot, J.; Fievet-Vincent, F. *J. Mater. Sci.* **1976**, *11*, 2267.

JP908548F